

On-Demand Activation of Photochromic Nanoheaters for High Color Purity 3D Printing

Authors: Alexander W. Powell¹, Alexandros Stavrinadis¹, Sotirios Christodoulou¹, Romain Quidant^{1,2}*, Gerasimos Konstantatos^{1,2}*

¹ICFO-Institut de Ciències Fòniques, The Barcelona Institute of Science and Technology, 08860 Castelldefels (Barcelona), Spain

²ICREA- Institució Catalana de Recerca i Estudis Avançats, 08810 Barcelona, Spain.

* Corresponding authors: gerasimos.konstantatos@icfo.eu, romain.quidant@icfo.eu

Abstract

The creation of white and multicoloured 3D-printed objects with high colour fidelity via powder sintering processes is currently limited by discolouration from thermal sensitizers used in the printing process. Here we circumvent this problem by using switchable, photochromic tungsten oxide nanoparticles, which are colourless even at high concentrations. Upon ultraviolet illumination, the tungsten oxide nanoparticles can be reversibly activated making them highly absorbing in the infrared. Their strong infrared absorption upon activation renders them efficient photothermal sensitizers that can act as fusing agents for polymer powders in sintering-based 3D printing. The WO₃ nanoparticles show fast activation times, and when mixed with polyamide powders they exhibit a heating-to-colour-change ratio greatly exceeding other sensitizers in the literature. Upon mixing with coloured inks, powders containing WO₃ display identical colouration to a pristine powder. This demonstrates the potential of WO₃ and photochromic nanoparticles in general as a new class of material for advanced manufacturing.

Keywords : 3D-Printing, photochromism, photothermal, tungsten oxide, laser sintering, plasmonic

In recent years a new generation of composite materials with advanced functionalities has arisen, opening up dynamic new frontiers in both conventional and advanced manufacturing by exploiting the unique properties of nanomaterials. The earliest example of this for 3D printed materials was the creation of nanocomposites through blending polymers with ceramic nanoparticles (NPs) such as alumina¹ and nanoclays² to improve the mechanical properties of the printed objects. More recently, carbon nanomaterials such as carbon nanorods³, graphene⁴, and core-shell structures⁵ have been used both to improve mechanical performance of 3D prints via laser sintering and to produce electrically conductive objects^{6-8,10} via a variety of methods. Silver nanoparticles have also been used to make antibacterial 3D prints⁹, gold nanoinks have been used to make 3D printed electrochemical reactors for catalysis¹⁰, and piezoelectric actuators and sensors have been printed with BaTiO₃ NP-polymer nanocomposite^{11,12}.

Another area in which nanomaterials have shown potential to disrupt current additive manufacturing (AM) technologies is in control over the aesthetic properties of the objects. Traditional 3D prints are printed in a monochrome and must be painted or dyed afterwards. There has been some experimentation with grading powders of different colour to produce a 'two tone' effect¹³ but this is a cumbersome process and more recent work has focused on inkjetting coloured inks into the powder during the printing process along with a thermal sensitizer using the 'High Speed Sintering' approach developed by Hopkinson et al¹⁴. However the colour fidelity of these prints is strongly dependent on the properties of the sensitizers used. Gold nanorods (GNRs) were shown to operate as a photothermal sensitizer to allow the rapid sintering of polymer powders into 3D objects using low-power light sources, and without significantly altering the aesthetic properties¹⁵. This was achieved by tuning the resonant absorption of the GNRs into the near infrared (NIR), leaving only weak absorption in the visible. Whilst this work showed excellent

results, there are some drawbacks to using gold nanorods as a photothermal sensitizer : GNRs are not stable at the very high temperatures required to sinter new high-performance polymers such as PEEK¹⁶ (melting temperature of 343 C¹⁷), but crucially GNRs intrinsically have weak absorption within the visible spectrum, which impacts on the colouration of prints when used in high concentrations, imposing intrinsic limits to the amount of GNRs one can use without affecting the color purity of the printed objects. In fact, this can be a problem for almost all plasmonic absorbers used for photothermal studies, in view of their absorption tail in the visible that becomes significant when the NPs are present in large quantities¹⁸⁻²⁴.

In order to reach high color purity in 3D prints, we posited that instead of using permanent absorbers to generate heat, the use of switchable absorbers would allow us to print objects with very high color purity and whiteness. This is important as a strongly coloured powder will limit the colour gamut available for a print, which can impact negatively on both the aesthetics and applications such as barcoding of prints²⁵. These would only possess strong optical absorption properties when they are needed to facilitate photothermal sintering, and would otherwise be transparent. Essentially, these switchable absorbers would act as programmable elements, which during the 3D printing process would be programmed, preferably optically, to switch ON and function as photothermal sensitizers, while later on they would switch OFF. To this end, we sought the use of photochromic materials, whose absorption can be altered via an external optical stimulus. In particular, we chose inorganic oxide semiconducting NPs due to their inherent stability at the elevated temperatures required in 3D printing²⁶.

One of the most promising of these materials is tungsten (VI) oxide, WO_3 , which has a strong absorption in the NIR that can be efficiently switched on and off using electricity (electrochromic)²¹ or ultraviolet radiation (photochromic)²⁷. Moreover, WO_3 is stable at high temperatures well above 400 C^{26,28}, and can be readily synthesized as nanoparticles using cheap reactants^{29,30}. In this work, we utilize for the first time the photochromic properties of WO_3 NPs to develop a 3D printing method that offers very high color purity and achieves white 3D printed objects via photothermal sintering with low cost NIR light sources.

To achieve this we synthesized WO_3 uncoated nanoparticles and mixed them with commercial AM powders to create a photochromic nanocomposite powder. We characterized the photochromic properties of these particles in ways not before applied to WO_3 NPs, and their behavior is found to agree with the general model of excitation seen in previous studies. We demonstrate the strong, rapid photochromic response of the WO_3 particles, and compare the photothermal heating and colouration of the powders to equivalent composite powders made with the industry standard carbon black (CB) as well as recently reported plasmonic nano-heaters based on GNRs. We demonstrate the sintering of these powders via a low power laser (a 1 W diode laser, compared to the ~40 W CO_2 lasers in traditional SLS machines³¹) to make 3D printed objects in order to demonstrate the colour contrast between the three sensitizers. Finally, we compare effect of the NP heat-sources on the hues of powders when mixed with coloured inks, highlighting the excellent utility of WO_3 for 3D printing white and finely coloured objects.

The photochromic effect of Tungsten oxide is due to the formation and decay of a hydrogen tungsten bronze (HWO_3) created by photo-induced interactions with the surrounding environment³². Briefly, the photo-generated electrons induced by UV-illumination decompose the water molecules on the surface of the NCs while reducing tungsten to W^{+5} oxidation state forming

HWO_3 near the surface, creating a doped hydrogen bronze^{27,32,33}. Upon illumination, these extra electrons in a WO_3 nanoparticle can interact with light in one of two ways. (i) Charge hopping between lattice sites of different W oxidation levels (the small polaron model)^{32,34,35}, (ii) absorption by free electrons and the excitation of surface plasmons³⁴⁻³⁶. The predominance of each mechanism is dependent on the substoichiometry of the particle and the level of hydrogen doping at any given time^{34,37}. This process has been shown to be highly reversible and stable over thousands of cycles³⁸.

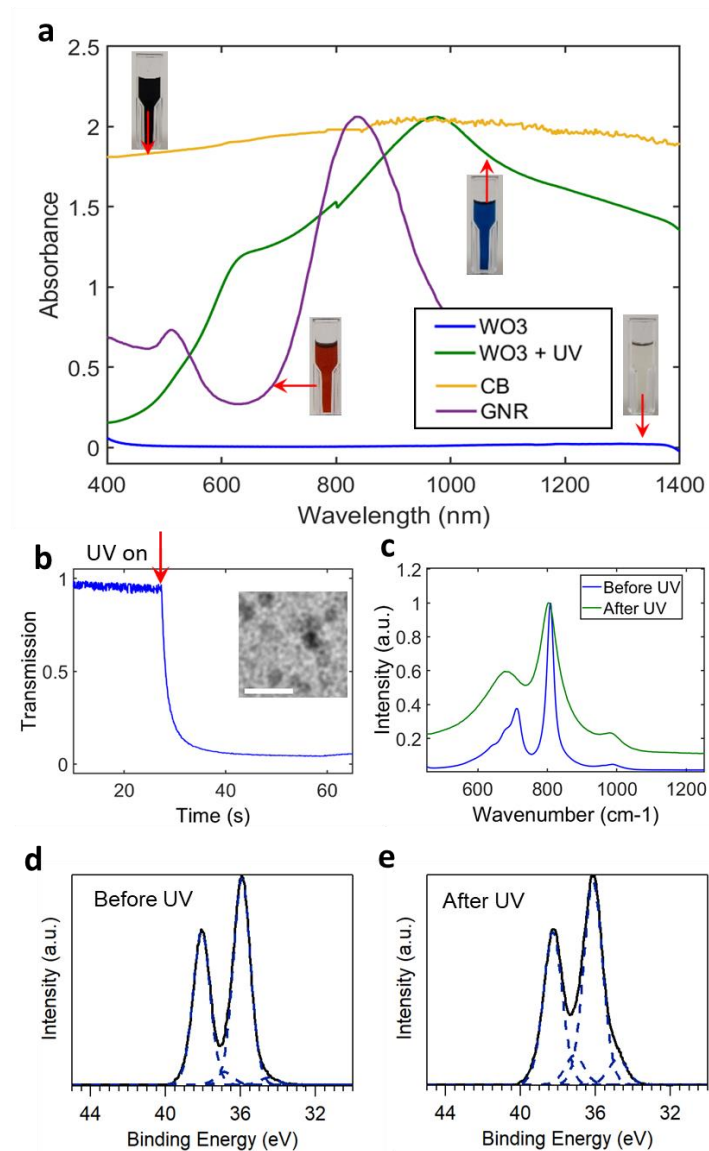


Figure 1: a) Absorption plots of GNRs, Carbon black, and WO₃ nanocrystals before and after UV illumination for 20 s. Photos of vials containing concentrated solutions of each material are also shown for clarity. b) The transmission of an 808 nm laser through a WO₃ solution while the samples is excited with UV light. The Inset shows a TEM image of the WO₃ NPs, the scale bar shows 20 nm. c) Raman spectra of the particles before and after illumination. XPS spectra from W 4f core level of WO₃ NCs before (d) and after illumination (e).

WO₃ NPs are synthesized following the procedure outlined by Brutsch et al²⁹ and were dispersed in water at a concentration of 3 g/L and their spectra are shown in Fig. 1a along with solutions of

CB and GNRs, next to photos of the solutions. For WO_3 the spectra is shown in the relaxed state, and the photoexcited state after illumination with ultraviolet (UV) light for 20 seconds. Whilst the carbon solution is completely black, the GNR and excited WO_3 spectra show a strong absorption band focused on a resonant value in the NIR. Dilute GNR solutions appear mostly transparent, but at high concentrations they have a distinct blood-red colour. The relaxed state of the WO_3 shows negligible absorption until the bandgap at wavelengths shorter than 400 nm, and the solution appears transparent in the visible, even at high concentrations. Upon UV photoexcitation the WO_3 shows strong absorption in the NIR with a tail in the visible strong enough to turn it a deep blue. This is a fully reversible and repeatable process, and after each excitation the sample reverts to its original colourless state. This effect occurs in dry samples as well as solutions (Figs S3, S4 & S6). In all cases environmental factors play an important role in determining the strength and speed of the photochromic response.

There are two distinct peaks present at 640 nm and 974 nm. Several previous studies have observed this double peak feature and have attributed the long wavelength peak to a plasmonic resonance in the nanoparticle, and the shorter wavelength peak to polaron hopping, although the exact position of peaks has been found to be highly dependent on the size and composition of the nanoparticles^{34,35}. Thus the potential of this material is already clear, if the strong absorption peak shown in Fig 1a can be switched on and off, then it is possible to achieve strong heating and sintering of powders via IR absorption, and later the absorption will switch off to leave the printed object uncoloured.

Fig. 1b shows the transmission dynamics of an 808 nm laser through a vial of 1 g/L WO_3 in H_2O , before and after excitation via a UV light, demonstrating the speed of this reaction. The transmission is reduced to 25% of its start point in, < 2 seconds and saturates at < 5% after 30s.

This demonstrates that the photochromic effect is excited very rapidly in the particles, and is a process compatible with 3D printing manufacturing. The inset of Fig 1b shows a TEM image of the WO₃ NPs. Several images were taken and a survey of NPs found their average size to be 6 ± 2 nm (See Fig. S2).

The origin of photochromism in WO₃ as described earlier is associated to its crystal structure and chemical composition being altered upon UV illumination in the presence of a hydrogen donor. We therefore performed Raman and X-ray Photoelectron spectroscopy to verify the mechanism at play in our NPs. Raman analysis in Fig. 1c shows two sharp peaks around 712 cm^{-1} and 809 cm^{-1} , both resulting from O–W⁶⁺–O stretching modes³². Upon UV illumination the peaks become significantly broader, which points to a decrease in WO₃ crystallinity, which is typical of the formation of the defect W⁵⁺ states in WO₃ and has been observed previously for electrochromic³⁹ and plasma-based excitation⁴⁰ of WO₃. We further confirm the photo-induced reduction of the tungsten by probing the W 4f core levels of the WO₃ NCs with X-ray photoelectron spectroscopy. In Fig. 1 d & e we show the W 4f core level spectra before and after UV illumination. The XPS spectra of the pristine WO₃ consisting of doublet peak due to spin-orbit coupling assigned as W 4f_{7/2} and W 4f_{5/2} with binding energies of 35.9 eV and 38.1 eV respectively, which corresponds to W⁺⁶. Furthermore, the XPS analysis of the W4f spectra after UV illumination suggest the reduction of the W⁺⁶ to W⁺⁵ which appears as an additional doublet peak shifted 1eV at lower energies in line with the previous reports studying plasma excitation.²⁹ We have not observed a complete reduction of the tungsten into W⁺⁵ oxidation state after UV-treatment which confirms that the photo-reduction mechanism takes place near the surface of the NCs as previously reported and agrees with the model of the formation of tungsten bronzes being responsible for the photochromic effect.³⁰

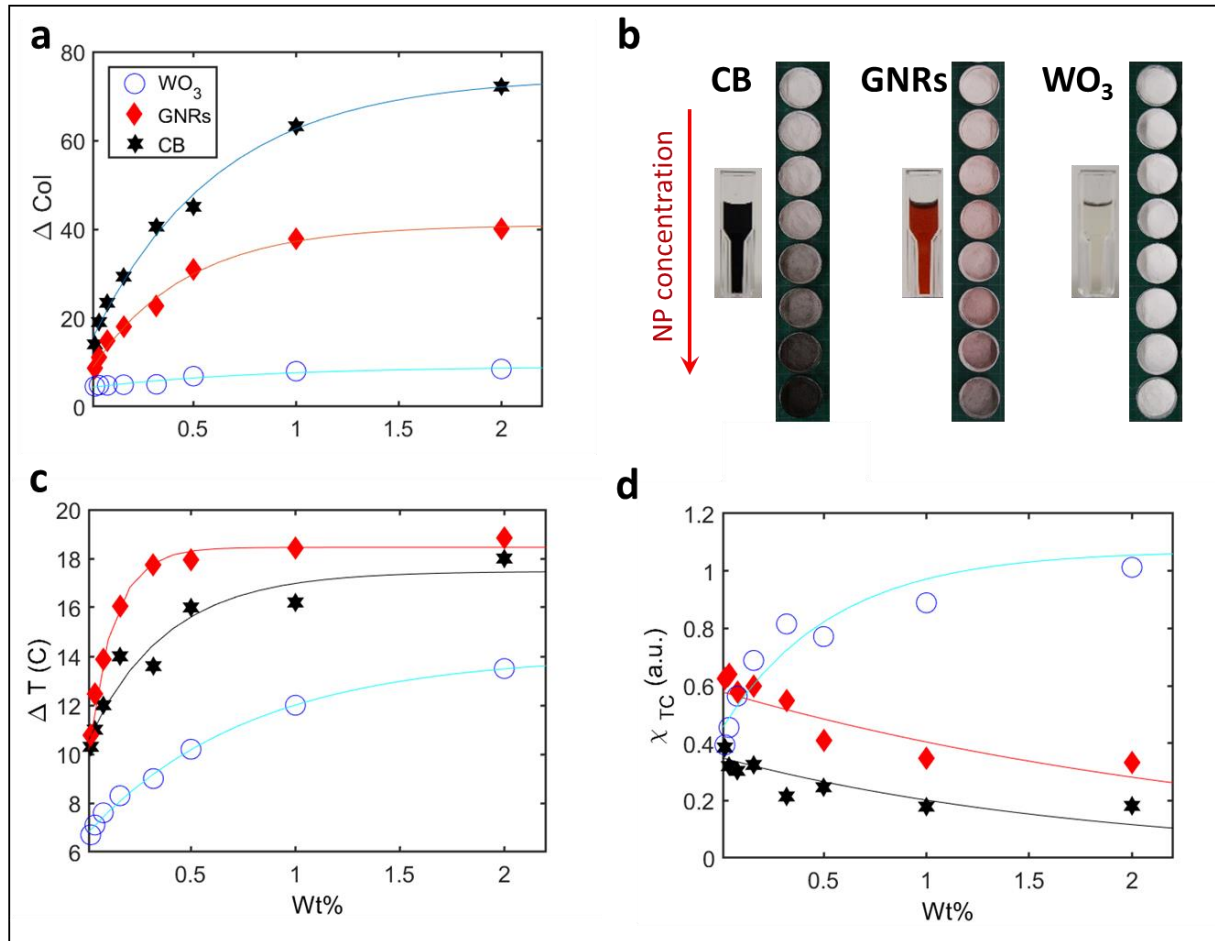


Figure 2: a) Colouration parameter ΔCol as a function of NP concentration for WO_3 -PA12, CB-PA12 and GNR-PA12 powder mixtures. b) Photographs of the different concentration powders used highlighting the effect of each nanoparticle on the colour. c) The heating, ΔT (increase in temperature from ambient values) for each concentration of powder under illumination from a 940 nm 100W LED array for CB and WO_3 and an 810 nm 100W LED array for GNR samples. The heating figure for the WO_3 -PA12 is given for the tungsten oxide in its active state after UV photoexcitation. d) The heating-to-colour-change ratio for each powder as a function of photothermal sensitizer concentration. Fit lines have been added as a visual aid.

The two key parameters for any photothermal sensitizer considered for 3-D printing are the degree to which they can enable the heating of a powder and the extent to which they change the colour of said powder and the final printed objects. In Figure 2a, the colour change from the pristine state,

ΔCol , caused by the addition of WO_3 , CB and GNR NPs to polyamide (PA12) powder with is shown as a function of NP concentration. Colouration is defined as $col = \sqrt{(a^*)^2 + (b^*)^2 + (L^*)^2}$ from the CIEL*a*b* scale, (See Fig. S10) and so $\Delta Col = \sqrt{(\Delta a^*)^2 + (\Delta b^*)^2 + (\Delta L^*)^2}$, with the base values of a^* , b^* and L^* are taken from pristine PA12. High values of ΔCol indicate a large change in the colour of the powder. It can be seen that even a tiny amount of CB has a marked impact on the powder colour - the addition of 0.02 % wt. of the powder leads to $\Delta Col = 14$, whereas the WO_3 has a negligible impact even at high concentrations, with a maximum value of $\Delta Col = 8.5$ for a 2 % wt. nanocomposite - 60 % the change in colour for 100x the sensitizer. This is illustrated visually in Fig. 2b, which shows that the WO_3 -PA12 powder remains white in its relaxed state for all concentrations used. Fig. S3 shows that as with the solutions in Fig. 1a, the WO_3 -PA12 powders and solid melted samples also take on a bluish colour after excitation with UV light, which then decays back to white after relaxation. GNR's have a smaller impact on the colouration than CB, but significantly more than WO_3 – and the ΔCol values lie almost at the midpoint of those of CB and WO_3 for all concentrations measured.

When illuminated at resonance with a 100 W LED array, the CB and GNRs heat more effectively than the WO_3 (in its active state after UV photoexcitation) at all concentrations, although the difference is less marked at higher concentrations, as shown in Fig. 2c. The GNRs have the strongest heating out of the three for all measured values. However the most important figure of merit is the heating that can be achieved for a change in colouration. The ideal photothermal sensitizer for colour 3DP will maximize heating and without altering the colouration. We therefore propose a new parameter, the heating-to-colour-change ratio, defined as : $\chi_{TC} = \Delta T / \Delta Col$. Fig. 2d shows that for CB, with increasing concentration, the change in colouration is stronger than the increase in heating, whereas for WO_3 , the change in colouration is negligible and so the increase

in heating dominates. The benefit of the photochromicity of WO_3 is clear here, as in the excited state they show a significant photothermal heating, but once this state has decayed they are almost colourless, producing the high χ_{TC} observed. The GNR's follow a similar trend to the CB, although with much higher χ_{TC} values. Very low concentrations of GNRs appear white and their very high heating allows for them to outperform low concentrations of WO_3 , but as seen in Fig. 2c the powder quickly darkens and takes on a pinkish tinge with increasing concentrations, and its heating-to-colour-change ratio is quickly overtaken by WO_3 for concentrations above 0.08 %wt. Powders with concentrations of GNRs greater than 0.02 %wt were found to have a pinkish tinge, especially notable when sintered, as seen in Fig. 3c.

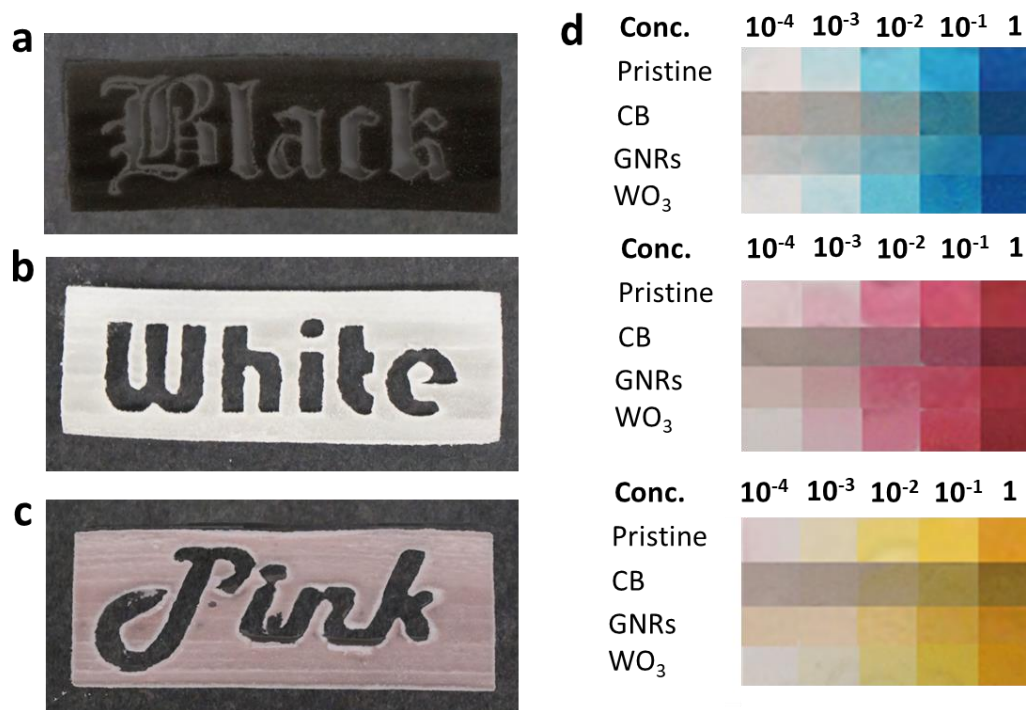


Figure 3: Laser sintered samples produced with 0.08 % wt. CB-PA12 powder (a), 1 % wt. WO_3 -PA12 powder (b), and 0.03 % wt. The samples are sintered rectangles with hollow letters. GNR-PA12 powder (concentrations chosen to give equivalent heating). (d) Photographs of different

concentrations of coloured ink dropped onto each of the three powders, highlighting the effect of the NP absorption on each primary colour.

We can therefore state that WO_3 is a more effective sensitizer than CB and GNRs in terms of the χ_{TC} parameter. Figure 3 illustrates the importance of this effect. A custom-made laser sintering bed, using a 1W 808 nm laser was used to sinter WO_3 -PA12, CB-PA12 and GNR-PA12 nanocomposite powders in exactly the same method that would be used in an SLS 3D printer (Fig. S9). The WO_3 -PA12 samples were illuminated via a UV lamp during sintering in order to maintain the highly absorbing excited state. The powders used to make these samples were mixed to have the same photothermal response at 808 nm, so in Fig. 3a the WO_3 has a concentration of 1 % wt, the CB has a concentration of 0.08% wt. and the GNRs have a concentration of 0.03 % wt in the powder. This shows the importance of considering both heating and colouration together. As the photothermal properties of the samples at the laser wavelength are identical, they will show the same ΔT for a given illumination, but the colour contrast between them is stark – the CB sample appears almost completely black and the GNR sample appears pink, whilst the WO_3 sample remains white.

The aesthetic impact of the photothermal sensitizers is also key for printing fully coloured objects, as the colour of the powder will obviously affect the colour of the finished prints. It is important to be able to print the full gamut of colours, as well as just in monochrome. This is investigated in Fig. 3d, which shows photos of PA12 powder in its pristine form and mixed in with WO_3 , CB and GNRs at the same concentrations as previously with various concentrations of red, blue and yellow inks dropped onto the powder. The ink was used as received for the most concentrated example,

and then diluted by a factor of 10 for each subsequent step, up until 10^{-4} . Their coloration was then measured with a colorimeter and plotted on the CIEL*a*b* scale.

Evidently, there is very little difference between the colouration of the inks on WO_3 and pristine powders. This is reflected in the ΔCol vs. ink concentration plots (See Fig. S11), where for every ink the traces from the WO_3 and the pristine powder are basically indistinguishable. For the CB powder however, it is clear from the photos in Fig. 3d that the colours are all darker and not as well defined as with the WO_3 . The ΔCol vs. concentration and L*a*b* plots (Fig. S11 & Fig. S12) show a significant difference between the colours on the CB powder compared to the others, and the lighter shades are simply not accessible due to the darkness of the powder. For the GNR's the stronger shades are almost indistinguishable from a pristine powder, but the lighter shades appear darker and redder, which would lead to a reduction of accuracy for lighter colours in printed objects. Thus the WO_3 powder shows a negligible change in hue compared to a pristine powder, even for very weak concentrations of inks, whereas the CB powder significantly restricts the available gamut to darker shades and the GNR powder reduces the accuracy of lighter shades.

In conclusion we have demonstrated that the use of photochromic tungsten oxide nanoparticles as a photothermal sensitizer has the potential to revolutionize high color quality 3D printing. WO_3 particles are easy and cheap to manufacture, show fast activation times, and demonstrate a heating-to-colour-change ratio far superior to other available sensitizers. When added to coloured inks, WO_3 reproduces even very pale shades perfectly in comparison to pristine powders. This work opens the door to a whole new class of nanomaterials for advanced manufacturing.

METHODS

Gold nanorods were synthesized in-house via the seed-mediated method of Nikoobackht & El-Sayed⁴², and coated in silica following Gorelikov and Matsuura⁴³. Carbon black powder was purchased from PlasmaChem. WO₃ was synthesized following the procedure of Brutsch et al²⁹ and dispersed in a concentrated form in deionized water. This method was selected as it produces small, uncoated nanoparticles with a high surface-to-volume ratio, which has been shown to be advantageous for maximizing the photothermal heating efficiency of nanoparticles^{44–46}, and will also aid the rate of photochromic excitation, which largely occurs at the particle surface^{32,34,37}. The small particle size also introduces quantum confinement effects which blueshift the absorption band edge out of the visible, leading to more transparent NPs (in their unexcited state). All of these effects will lead to a greater heating-to-colour-change ratio for the WO₃-PA12 composites, which is highly desirable

Absorption measurements were obtained from particles in solution using a Cary 5000 spectrometer. TEM measurements were carried out in a JEOL JEM-2100 LaB6 transmission electron microscope operating at 200kV. Raman spectra were collected using a Renishaw InVia MicroRaman spectrometer, exciting the samples with a 100 mW diode laser at $\lambda=532$ nm, using a $\times 50$ magnification microscope objective. XPS measurements were performed with a Phoibos 150 analyzer (SPECS GmbH) in ultra-high vacuum conditions using a monochromatic Kalpha x-ray source (1486.74eV). The photochromic excitation speed tests were carried out using a custom setup defined in Figure S7.

The NPs were diluted in ethanol then mixed with pristine PA12 powder from Advanc3Dmaterials at differing wt % concentrations then dried in an oven at 60 C overnight. After drying powders were sieved prior to printing. For measuring the effects of the NPs on the colour of powders, various concentrations of commercially available inks were drop-cast onto the powders and the colouration measured with a colorimeter.

To perform the comparative tests between the different sensitizers, the powder, small samples of powder in a shallow aluminium holder were illuminated by a 100W 810 nm or 100W 940 nm LED array from Shenzhen Hanhua Opto Co. The temperature of all samples was measured using a FLIR ax5 thermal camera, and the colour tests were performed using a PCE instruments PCE-CSM 4 colorimeter.

To sinter the printed shapes in Fig. 3, a custom made laser writing setup was used, as described previously¹⁵. Samples were preheated by a hotplate below and IR lamps from above in order to mimic the conditions in a SLS printer. The bulk of the powder was heated to 150C using the hotplate and then the top layer heated to 172.5 C using the lamps. A Dymax Bluewave 200 UV lightsource was used to illuminate the WO₃-PA12 sample during this process to maintain the nanoparticles in their photoexcited state. A 1W 808 nm diode laser from Thorlabs was used to sinter the powder and define the shape of the prints.

Supporting Information

Showing illustrations of the experiments used and additional results on the colouration of powders after the addition of the inks.

Acknowledgements

The authors acknowledge financial support from the European Community's Seventh Framework Program under grant QnanoMECA (64790), Fundació Privada Cellex, the program CERCA, the Spanish Ministry of Economy and Competitiveness, through the "Severo Ochoa" Programme for Centres of Excellence in R&D (SEV-2015-0522) and grant FIS2016-80293-R, the European Research Council (ERC) under the European Union's Horizon 2020 research and innovation programme (grant agreement No 725165), the Spanish Ministry of Economy and Competitiveness (MINECO) and the "Fondo Europeo de Desarrollo Regional" (FEDER) through grant TEC2017-88655-R.

References

1. Warnakula, A. & Singamneni, S. Selective Laser Sintering of Nano Al₂O₃ Infused Polyamide. *Materials (Basel)*. **10**, 864 (2017).
2. Almansoori, A., Majewski, C. & Rodenburg, C. Nanoclay/Polymer Composite Powders for Use in Laser Sintering Applications: Effects of Nanoclay Plasma Treatment. *JOM* (2017), 69, pp. 2278–2285
3. Bai, J. *et al.* Thermal Influence of CNT on the Polyamide 12 Nanocomposite for Selective Laser Sintering. *Molecules* **20**, 19041–19050 (2015).
4. Chen, B., Berretta, S., Evans, K., Smith, K. & Ghita, O. A primary study into graphene/polyether ether ketone (PEEK) nanocomposite for laser sintering. *Appl. Surf. Sci.* **428**, 1018–1028 (2018).
5. Chen, B. *et al.* Fabrication of nanocomposite powders with a core-shell structure. *Compos. Sci. Technol.* **170**, 116–127 (2019).
6. Zhang, Q. *et al.* 3D Printing of Graphene Aerogels. *Small* **12**, 1702–1708 (2016).
7. Zhang, D. *et al.* Fabrication of highly conductive graphene flexible circuits by 3D

- printing. *Synth. Met.* **217**, 79–86 (2016).
8. Gnanasekaran, K. *et al.* 3D printing of CNT- and graphene-based conductive polymer nanocomposites by fused deposition modeling. *Appl. Mater. Today* **9**, 21–28 (2017).
 9. Tiimob, B. J. *et al.* Nanoengineered Eggshell–Silver Tailored Copolyester Polymer Blend Film with Antimicrobial Properties. *J. Agric. Food Chem.* (2017), 65, 9, 1967-1976
 10. Zhu, C. *et al.* Toward digitally controlled catalyst architectures: Hierarchical nanoporous gold via 3D printing. *Sci. Adv.* **4**, eaas9459 (2018).
 11. Kim, K. *et al.* 3D Optical Printing of Piezoelectric Nanoparticle–Polymer Composite Materials. *ACS Nano* 2014, 8, 10, 9799-9806
 12. Chen, Z. *et al.* 3D printing of piezoelectric element for energy focusing and ultrasonic sensing. *Nano Energy* **27**, 78–86 (2016).
 13. Loh, G. H., Pei, E., Harrison, D. & Monzón, M. D. An overview of functionally graded additive manufacturing. *Additive Manufacturing* **23**, 34–44 (2018).
 14. Hopkinson, N. & Erasenthiran, P. High Speed Sintering—Early Research Into a New Rapid Manufacturing Process. in *International Solid Freeform Fabrication Symposium* 312–320 (2004).
 15. Powell, A. W., Stavrinadis, A., Miguel, I. de, Konstantatos, G. & Quidant, R. White and Brightly Colored 3D Printing Based on Resonant Photothermal Sensitizers. *Nano Lett.* (2018) 18, 11, 6660-6664
 16. Wagner, T., Höfer, T., Knies, S. & Eyerer, P. Laser Sintering of High Temperature Resistant Polymers with Carbon Black Additives. *Int. Polym. Process.* **19**, 395–401 (2004).
 17. Kroh, M., Bonten, C. & Eyerer, P. Improvement of mechanical properties by additive assisted laser sintering of PEEK. in *AIP Conference Proceedings* 724–727 (2014). doi:10.1063/1.4873879
 18. Jiang, R., Cheng, S., Shao, L., Ruan, Q. & Wang, J. Mass-Based Photothermal Comparison Among Gold Nanocrystals, PbS Nanocrystals, Organic Dyes, and Carbon Black. *J. Phys. Chem. C* **117**, 8909–8915 (2013).
 19. Thakore, V., Tang, J., Conley, K., Ala-Nissila, T. & Karttunen, M. Thermoplasmonic Response of Semiconductor Nanoparticles: A Comparison with Metals. *Adv. Theory Simulations* **2**, 1800100 (2019).
 20. Ding, X. *et al.* Surface Plasmon Resonance Enhanced Light Absorption and Photothermal Therapy in the Second Near-Infrared Window. *J. Am. Chem. Soc.* **136**, 15684–15693 (2014).
 21. Wang, Y. *et al.* Comparison Study of Gold Nanohexapods, Nanorods, and Nanocages for Photothermal Cancer Treatment. *ACS Nano* **7**, 2068–2077 (2013).
 22. Faucheaux, J. A., Stanton, A. L. D. & Jain, P. K. Plasmon resonances of semiconductor

- nanocrystals: Physical principles and new opportunities. *Journal of Physical Chemistry Letters* **5**, 976–985 (2014).
23. Scotognella, F. *et al.* Plasmonics in heavily-doped semiconductor nanocrystals. *Eur. Phys. J. B* **2013** 864 **86**, 1–13 (2013).
 24. Yu, N. *et al.* Dopant-dependent crystallization and photothermal effect of Sb-doped SnO₂ nanoparticles as stable theranostic nanoagents for tumor ablation. *Nanoscale* **10**, 2542–2554 (2018).
 25. Huang, W. & Mow, W. H. Picode: 2D barcode with embedded picture and vicode: 3D barcode with embedded video :Innovative system for transmitting data from display to camera. in *Proceedings of the Annual International Conference on Mobile Computing and Networking, MOBICOM* 139–141 (ACM Press, 2013).
 26. Szilágyi, I. M. *et al.* Thermal stability of hexagonal tungsten trioxide in air. *J. Therm. Anal. Calorim.* (2008). doi:10.1007/s10973-007-8601-y
 27. Bechinger, C., Burdis, M. S. & Zhang, J. G. Comparison between electrochromic and photochromic coloration efficiency of tungsten oxide thin films. *Solid State Commun.* (1997). 101, 10, 753-756
 28. Romanyuk, A. *et al.* Thermal stability of tungsten oxide clusters. *J. Phys. Chem. C* **112**, 11090–11092 (2008).
 29. Brütsch, L. *et al.* Surfactant-free synthesis of sub-stoichiometry tungsten oxide nanoparticles and their use as anode buffer layers in organic solar cells. *Solid State Sci.* **69**, 50–55 (2017).
 30. Mattox, T. M., Bergerud, A., Agrawal, A. & Milliron, D. J. Influence of shape on the surface plasmon resonance of tungsten bronze nanocrystals. *Chem. Mater.* **26**, 1779–1784 (2014).
 31. Brandt, M. *Laser Additive Manufacturing Materials, Design, Technologies, and Applications*; Brandt, M. Ed.; Woodhead Publishing : Duxford, UK, 2017.
 32. Dejournett, T. J. & Spicer, J. B. The influence of oxygen on the microstructural, optical and photochromic properties of polymer-matrix, tungsten-oxide nanocomposite films. *Sol. Energy Mater. Sol. Cells* (2014) 120, 102-108
 33. Sun, M., Xu, N., Cao, Y. W., Yao, J. N. & Wang, E. G. Nanocrystalline tungsten oxide thin film: Preparation, microstructure, and photochromic behavior. *J. Mater. Res.* (2000), 15, 4, 927-933
 34. Adachi, K. & Asahi, T. Activation of plasmons and polarons in solar control cesium tungsten bronze and reduced tungsten oxide nanoparticles. *J. Mater. Res.* (2012). 27, 6, 965-970
 35. Li, N. *et al.* A plasmonic non-stoichiometric WO₃-: X homojunction with stabilizing surface plasmonic resonance for selective photochromic modulation. *Chem. Commun.* (2018). 54(41):5241-5244

36. Manthiram, K. & Alivisatos, A. P. Tunable localized surface plasmon resonances in tungsten oxide nanocrystals. *J. Am. Chem. Soc.* (2012). 134, 9, 3995-3998
37. Salje, E. & Güttler, B. Anderson transition and intermediate polar on formation in WO₃-xtransport properties and optical absorption. *Philos. Mag. B Phys. Condens. Matter; Stat. Mech. Electron. Opt. Magn. Prop.* (1984). 50, 5, 607-620
38. Heo, S., Kim, J., Ong, G. K. & Milliron, D. J. Template-Free Mesoporous Electrochromic Films on Flexible Substrates from Tungsten Oxide Nanorods. *Nano Lett.* **17**, 5756–5761 (2017).
39. Lee, S. H. *et al.* Raman spectroscopic studies of electrochromic α -WO₃. *Electrochim. Acta* (1999). 44(18):3111-3115
40. Rahimnejad, S. *et al.* Enhancement of the photocatalytic efficiency of WO₃ nanoparticles via hydrogen plasma treatment. *Mater. Res. Express* (2015). 1, 4, 045044
41. Xie, F. Y. *et al.* XPS studies on surface reduction of tungsten oxide nanowire film by Ar + bombardment. *J. Electron Spectros. Relat. Phenomena* (2012). 185, 3-4, 112-118.
42. and, B. N. & El-Sayed*, M. A. Preparation and Growth Mechanism of Gold Nanorods (NRs) Using Seed-Mediated Growth Method. *Chemisre Mater.* **15**, 1957–1962 (2003).
43. Gorelikov, I. & Matsuura, N. Single-Step Coating of Mesoporous Silica on Cetyltrimethyl Ammonium Bromide-Capped Nanoparticles. *Nano Lett.* **8**, 369–373 (2007).
44. Waller, M. R. *et al.* Single-crystal tungsten oxide nanosheets: Photochemical water oxidation in the quantum confinement regime. *Chem. Mater.* **24**, 698–704 (2012).
45. Cong, S., Tian, Y., Li, Q., Zhao, Z. & Geng, F. Single-Crystalline Tungsten Oxide Quantum Dots for Fast Pseudocapacitor and Electrochromic Applications. *Adv. Mater.* **26**, 4260–4267 (2014).
46. Jiang, K., Smith, D. A. & Pinchuk, A. Size-dependent photothermal conversion efficiencies of plasmonically heated gold nanoparticles. *J. Phys. Chem. C* **117**, 27073–27080 (2013).

ToC

